ICA: Isotropic Conductive Adhesives (☼)

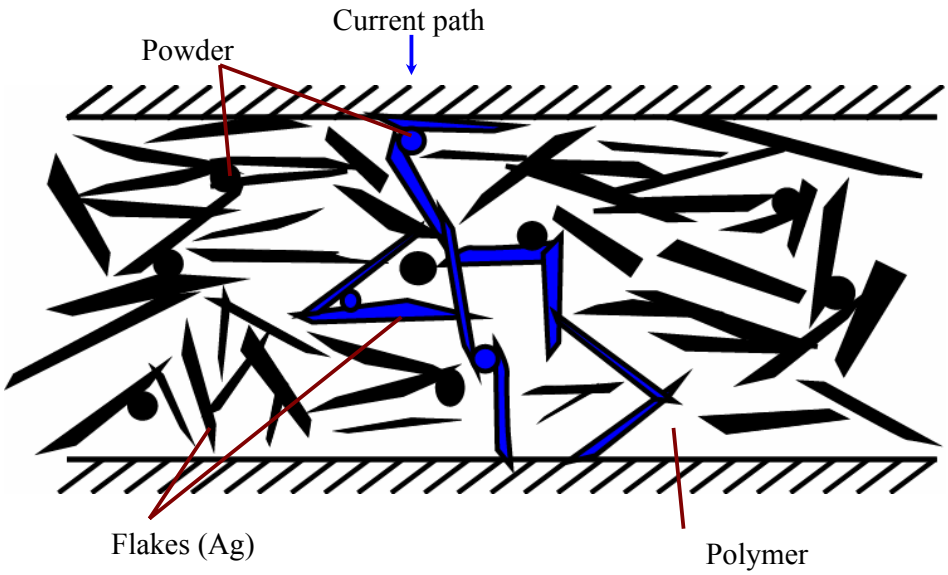

ICA Smart Cards & RF ID (☼)

(IZM-Berlin)

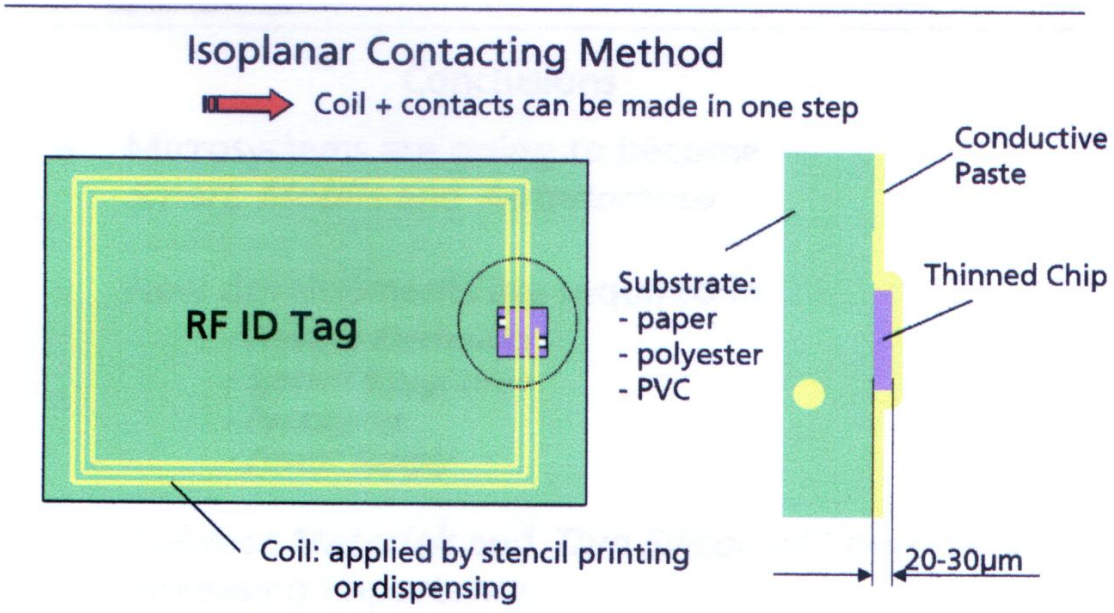

3.2 Calculation Results: Degree of Cure vs. Time for 3 Adhesives (☼)

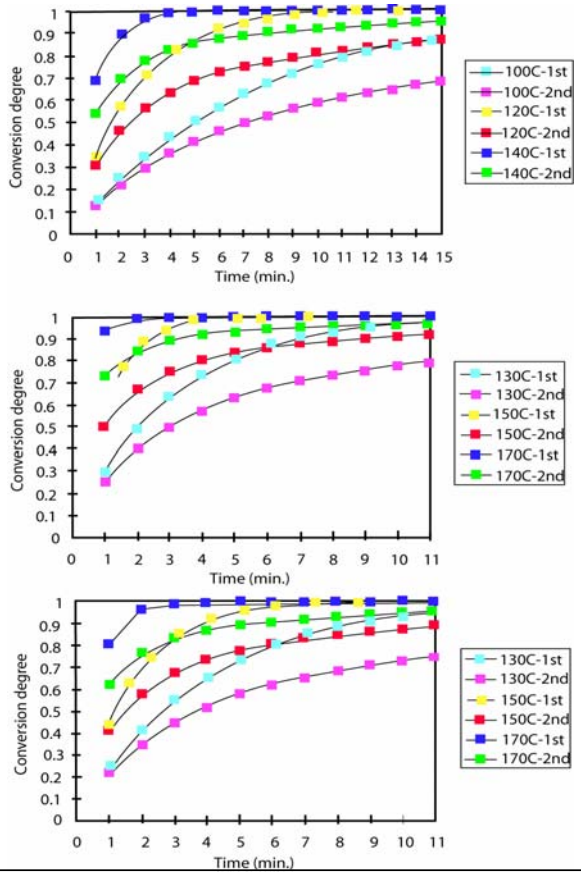

Cure Modeling (☼)

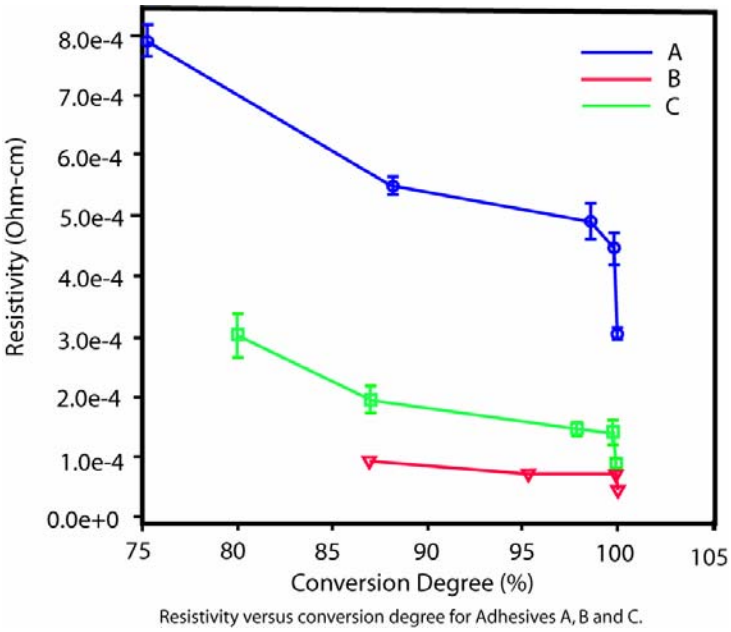

Resistivity versus conversion degree for Adhesives A, B and C.

- Simple cure models work well
- Manufacturer profiles -> incomplete cure

3.3 Shrinkage vs Degree of Cure

Characterization Technique (☼)

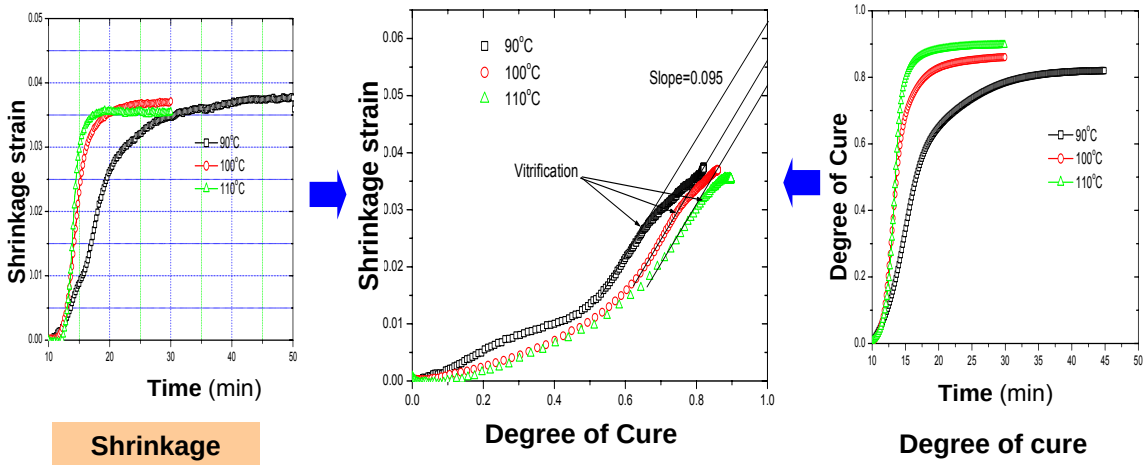

Shrinkage measurement (slide 14)

Shrinkage Strain Vs Degree of Cure

Degree of cure measurement (slide 9)

Slide courtesy of E. H. Wong

Cure Shrinkage vs Degree of Cure

Characteristics

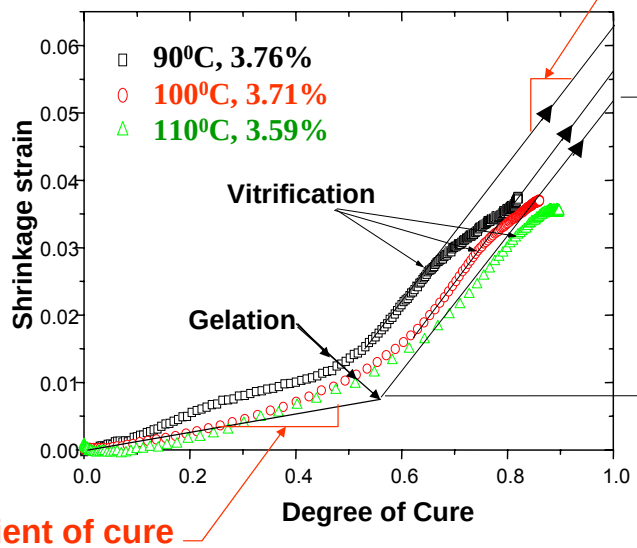

Coefficient of cure shrinkage (CCS_2) – **almost independent of cure temperature**

≈4.2%
Almost independent of cure temperature

Coefficient of cure shrinkage (CCS_1)

(☼)

Slide courtesy of E. H. Wong

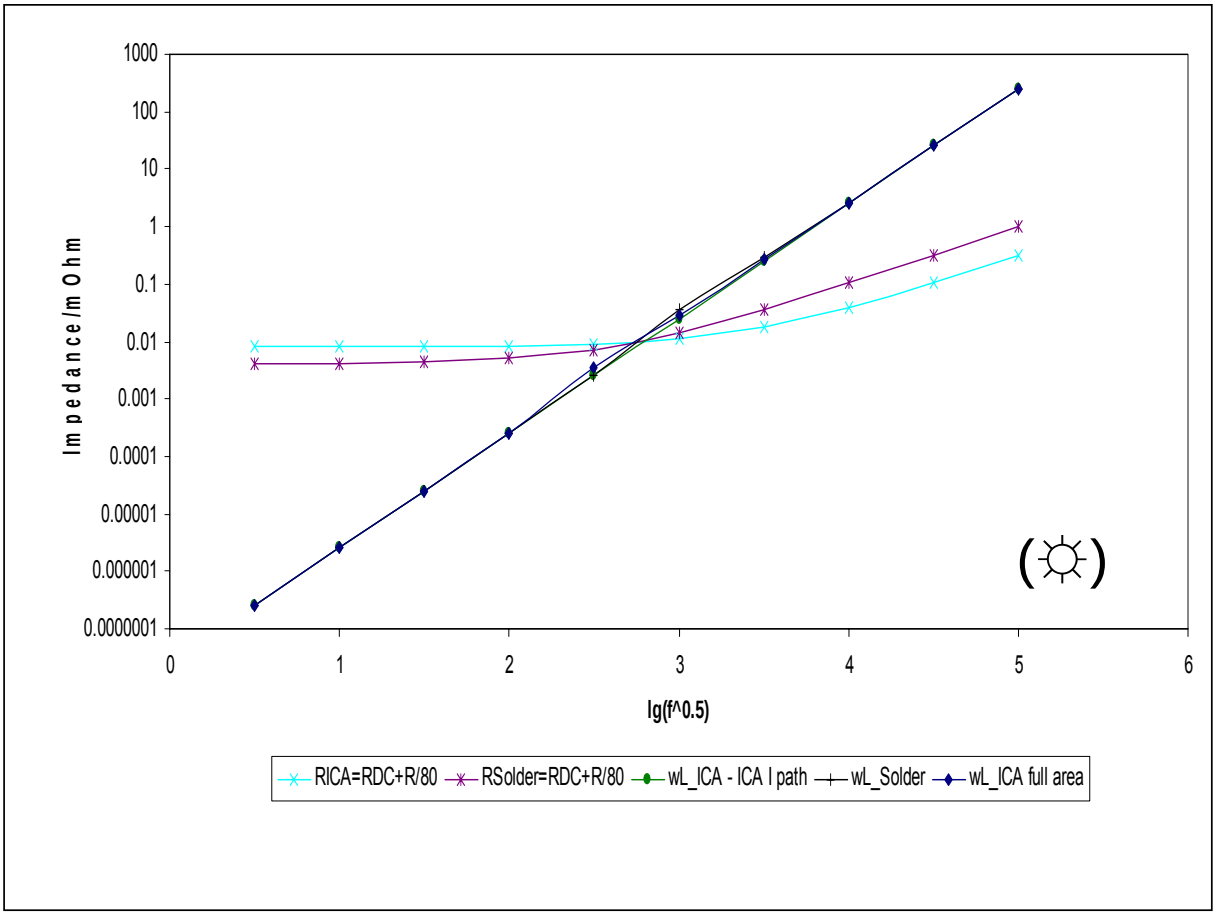

PAE2 thermoplastic for lower moisture absorption. But poor contact resistance stability due to poor adhesion. Add "coupling agent" (e.g. CA4) to improve. But note correlation with surface roughness. [Liong/Wong (ECTC 2002)]

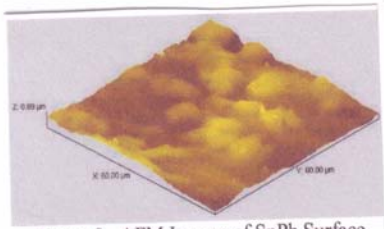

Figure 9. AFM Images of SnPb Surface

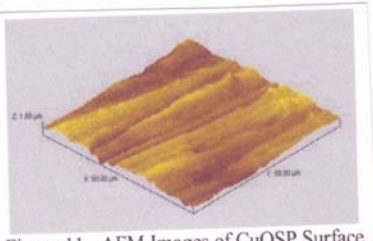

Figure 11. AFM Images of CuOSP Surface

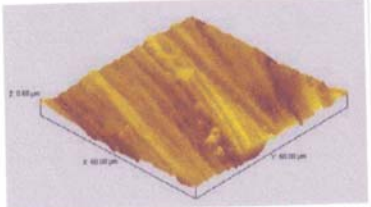

Figure 10. AFM Images of Sn Surface

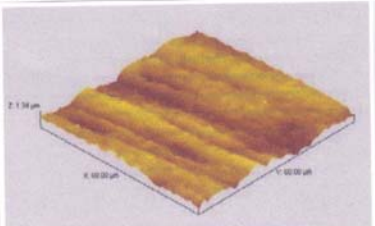

Figure 12. AFM Images of NiAu Surface

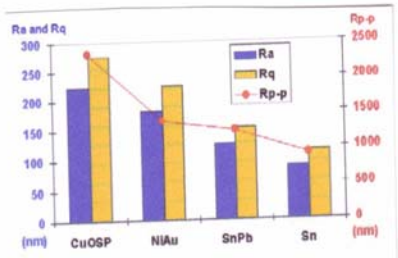

Figure 8. AFM Data Summary

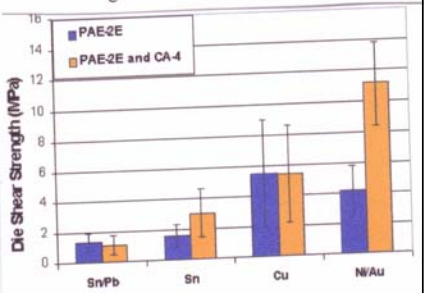

Figure 17. Adhesion Data of PAE-2E with CA-

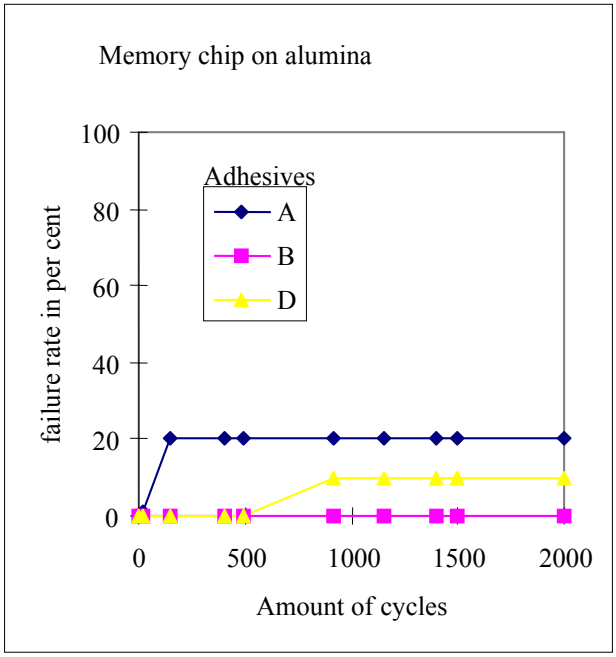

Failure rate in thermal cycling (-40...+125 °C).
Memory chips were bonded onto alumina substrates.

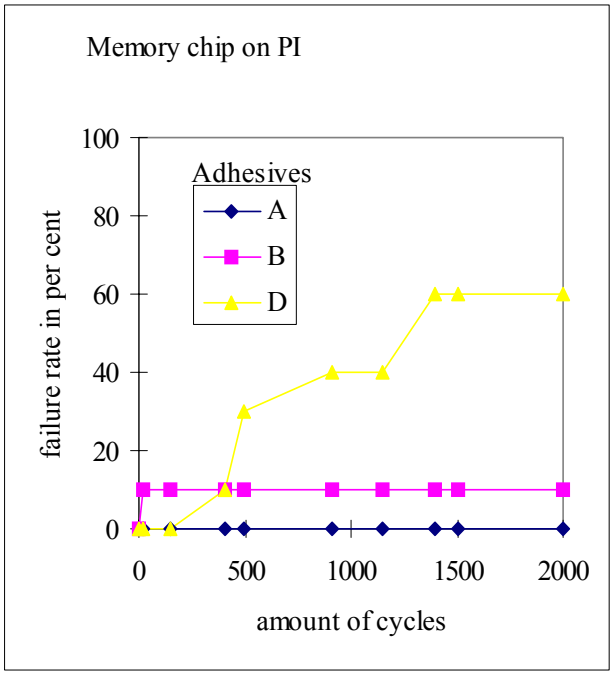

Failure rate in thermal cycling (-40...+125 °C).
Memory chips were bonded onto polyimide substrates.

Extracted Resistance (☼)

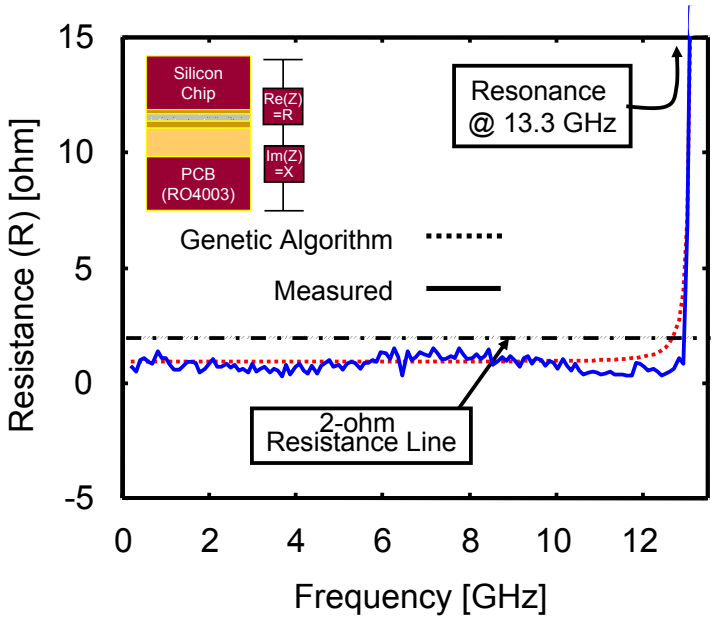

Extracted Reactance (☼)

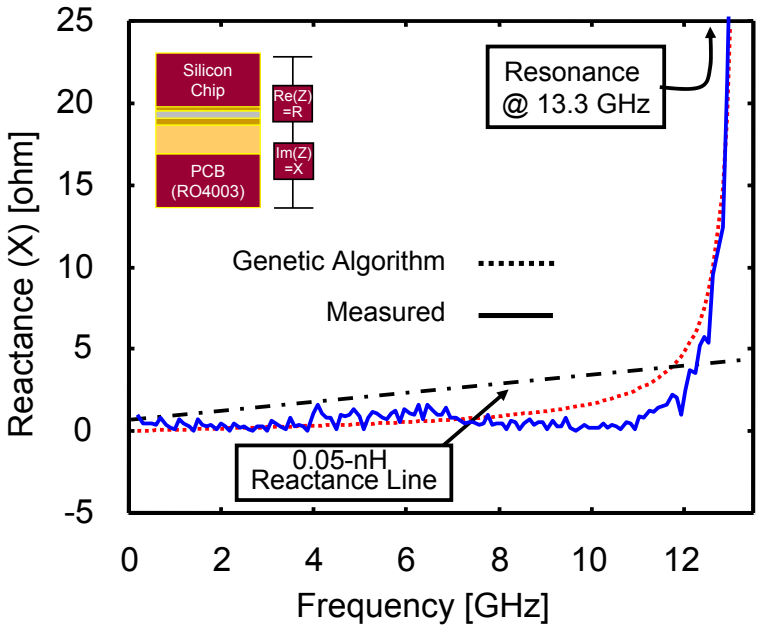

Measured Time-Domain Transmission through ACF (☼)

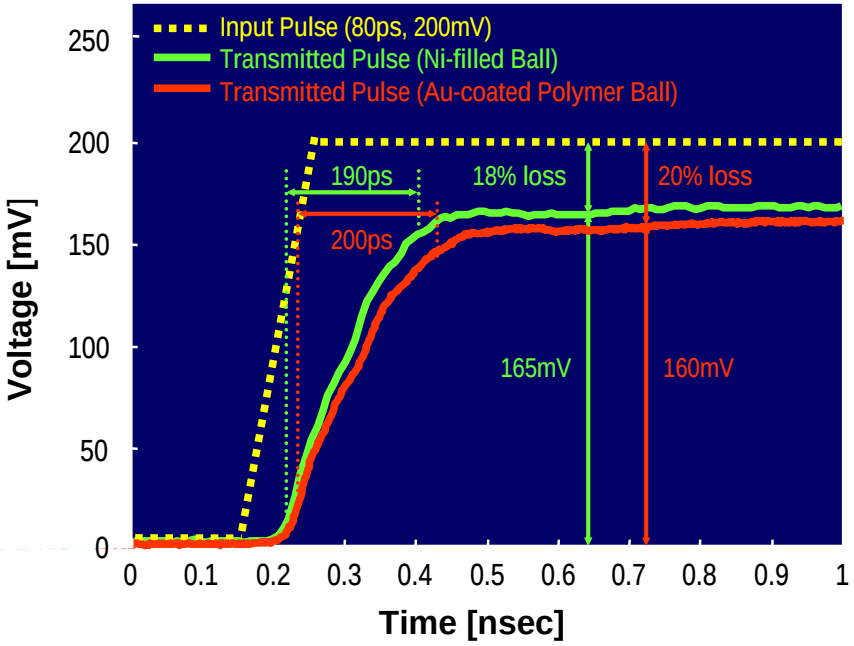

4.2 Thermal Conductivity

[Yim et al, ECTC'06]

(☼)

ACP-3 has <1μm SiC filler added to Ni (ACP-1)

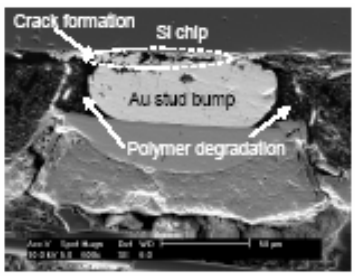

Fig. 6. Cross sectional SEM pictures at Au stud bumps joints by conventional ACA after current stressing reliability test.

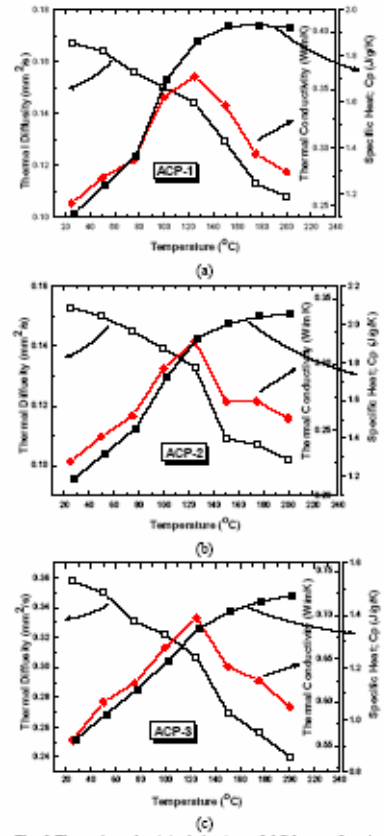

Fig. 2 Thermal conductivity behaviors of ACAs as a function of temperature for three ACA materials; (a) Ni-filled ACA, (b) Au-coated polymer ball-filled ACA and (c) Ni-filled and thermally conductive ACA.

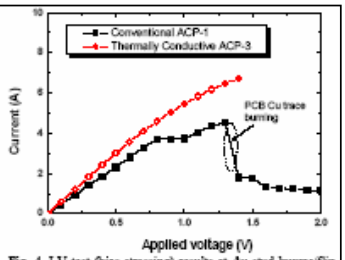

Fig. 4. I-V test (bias stressing) results at Au stud bumps/flip chip joints by conventional ACA and thermally conductive ACA.

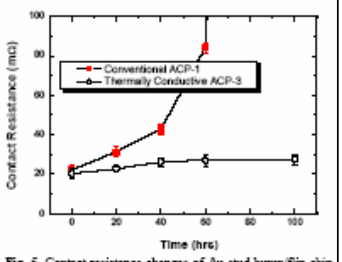

Fig. 5. Contact resistance changes of Au stud bump/flip chip joints using conventional ACA and thermally conductive ACA after 20, 40, 60, 100 hours under current stressing.

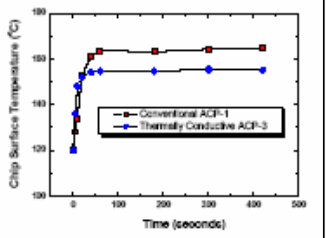

Fig. 7 Chip surface temperature of flip chip assemblies using conventional and thermally conductive ACAs as a function of current stressing time.

ACF COG Warpage of LCD Modules

[Xie et al, ECTC'06] (☼)

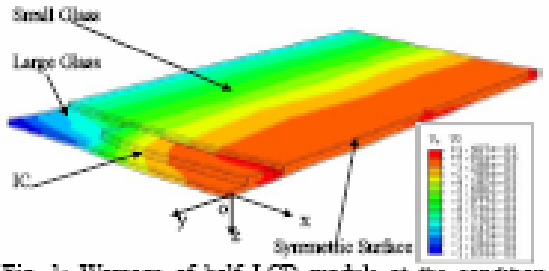

Fig. 1: Warpage of half LCD module at the condition of BP130N/BHT280°C/GST120°C with scale factor of 50

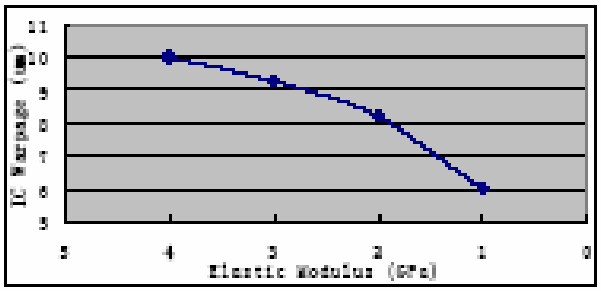

Fig. 3: Effect of ACF elastic modulus on IC warpage

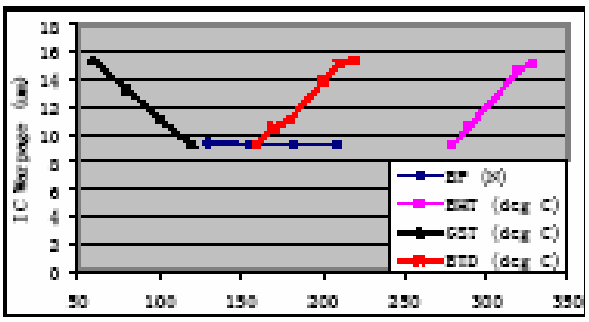

Fig. 2: Effect of bonding parameters on IC warpage

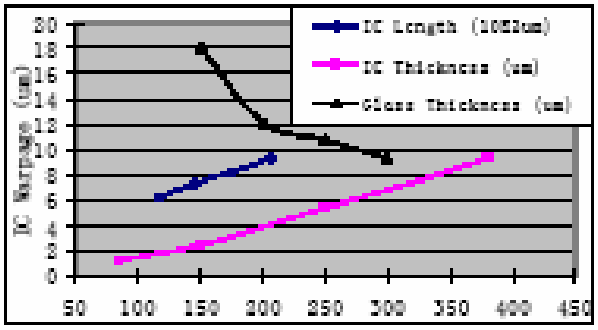

Fig. 4: Effect of geometry of IC and glass on IC warpage

ACF COG Warpage of LCD Modules

[Xie et al, ECTC'06] (☼)

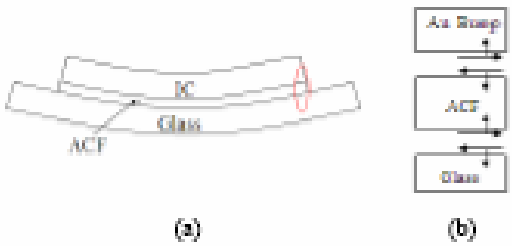

Fig. 5: (a) LCD module warpage behavior and (b) zoom-in local stress distribution of region highlighted in (a).

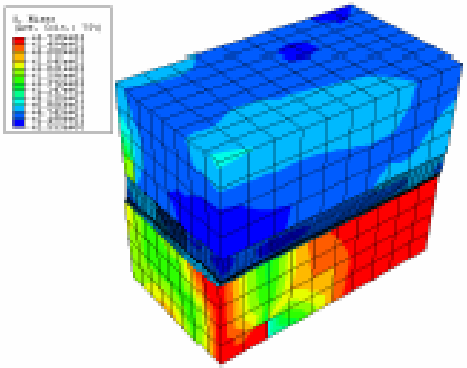

Fig. 7: Von Mises distribution in the local model of outermost output bump area

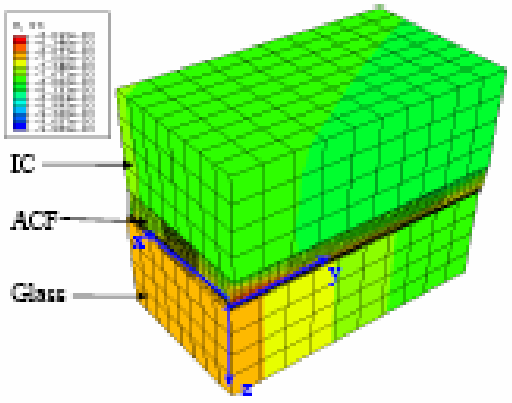

Fig.6: Warpage of the local model of outermost output bump area

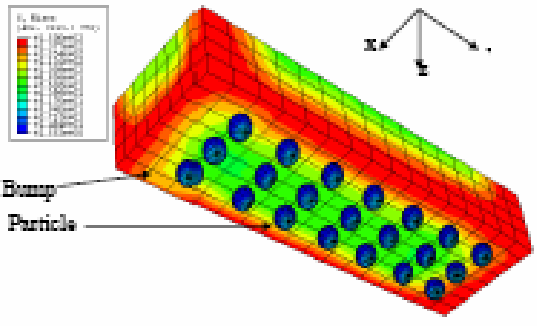

Fig.8: Von Mises distribution in gold bump and particles

Rupture/Resistance Modeling (☼)

[Xie et al, ECTC'06]

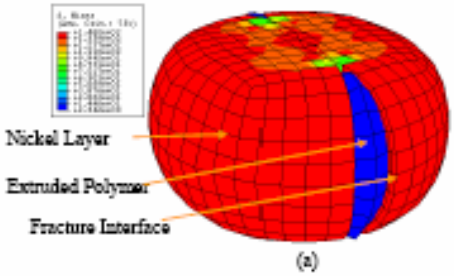

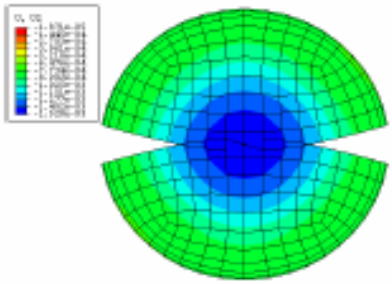

Fig. 16: Deformation of conductive particle model at bonding force 77.3MPa with (a) 3D view and (b) top view

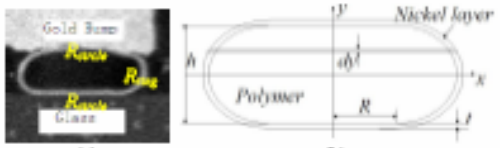

Fig. 17: (a) Components of particle resistance in a single particle and (b) profile of nickel coated polymer particle

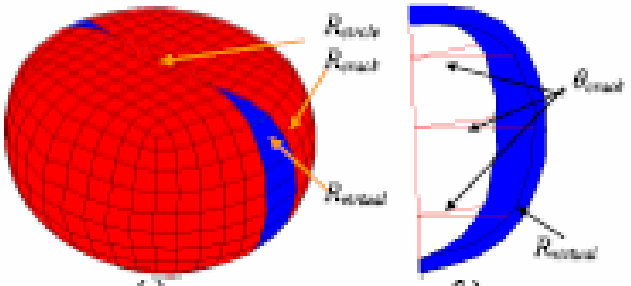

Fig. 18: Schematic of (a) particle resistance components with cracks and (b) virtual resistance

6.2 Nanowire ACF

[Lin et al (ITRI), ECTC'05] (☼)

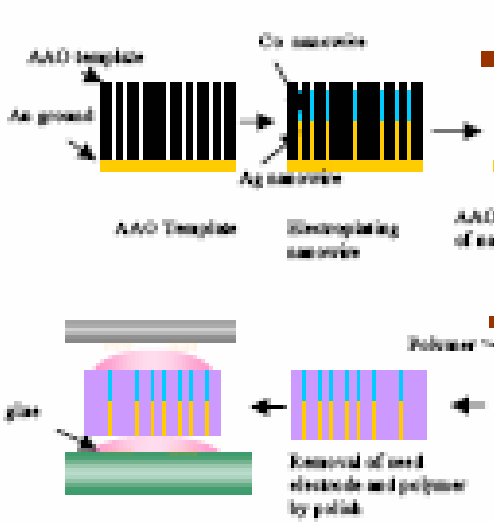

Fig. 1 Process Flow of Nanowire Conductive Film

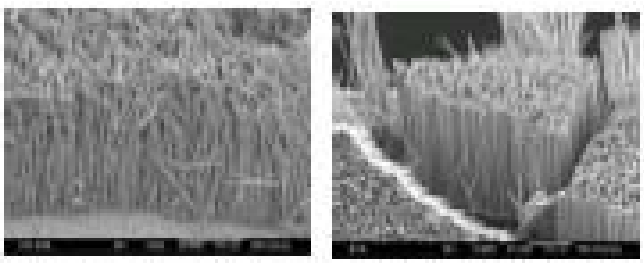

Fig. 4 Ag (Left) and Cobalt (Right) Nanowires

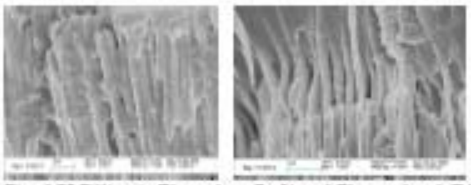

Fig. 6 PI Filling in Electroless (Left) and Electroplated (Right) Ag Nanowires Arrays

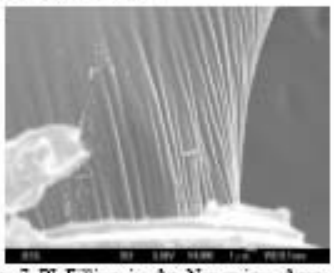

Fig. 7 PI Filling in Ag Nanowires Array after Fatty Acid Surface Treatment

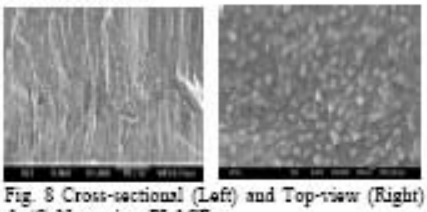

Fig. 8 Cross-sectional (Left) and Top-view (Right) SEM of Ag/CoNanowires-PI ACF

Adhesive Layer Thermal Transient: ICA Flip-chip, 1sec (☼)

Transient thermal temperature response after 1 second in a flip-chip mounted with isotropically electrically conductive adhesive joints seen through the pad row

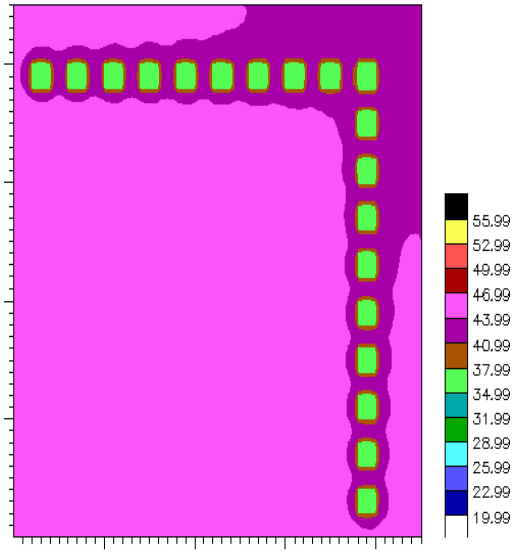

Thermal management, cont. (☼)

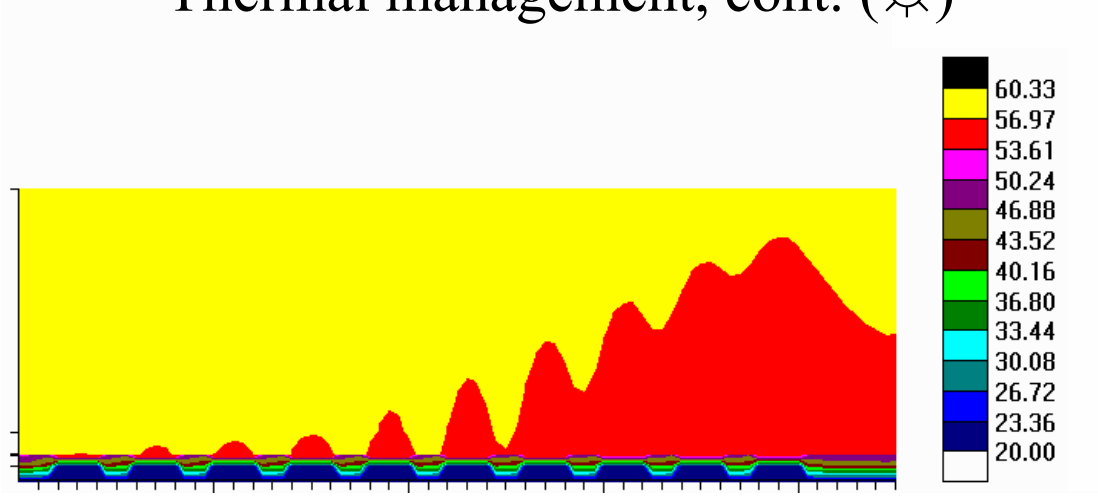

Transient thermal temperature response after 1 second in a flip-chip mounted with isotropically electrically conductive adhesive joints seen in the adhesive joint layer